3936 *Biochemistry* **2009,** *48,* 3936–3945
DOI:10.1021/bi900029j

BIOCHEMISTRY
including biophysical chemistry & molecular biology
Article

Evidence for a Ca^{2+}-Specific Conformational Change in Avian Thymic Hormone, a High-Affinity *β*-Parvalbumin†

Anmin Tan and Michael T. Henzl*

Department of Biochemistry, University of Missouri, Columbia, Missouri 65211

Received January 8, 2009. Revised Manuscript Received March 16, 2009

ABSTRACT: Named for the capacity to stimulate differentiation and maturation of T-cell precursors, avian thymic hormone (ATH) is nonetheless a *β*-parvalbumin that is also expressed in the avian retina. With Ca^{2+}- and Mg^{2+}-binding constants in excess of 10^8 and 10^4 M^{-1}, respectively, both EF-hand motifs qualify as Ca^{2+}/Mg^{2+} sites. However, whereas addition of either apo- or Mg^{2+}-bound ATH to 1,8-anilinonaphthalenesulfonic acid (ANS) causes a large increase in quantum yield and a pronounced blue shift, addition of the Ca^{2+}-bound protein is without effect. These observations suggest that apo- and Mg^{2+}-bound ATH adopt conformations distinct from the Ca^{2+}-bound protein, exposing apolar surface for interaction with ANS. Differential scanning calorimetry (DSC) data imply that unfolding of apo-ATH is accompanied by diminished exposure of apolar surface, relative to Ca^{2+}-free rat *β*-PV, perhaps due to greater solvent-accessible apolar surface in the native form. The fluorescence and DSC results, considered together, may indicate that the AB and CD-EF domains of ATH are not tightly associated in the absence of bound Ca^{2+}. Consistent with this idea, sedimentation velocity data reveal that the apo- and Mg^{2+}-bound forms of ATH show greater departures from spherical symmetry than the Ca^{2+}-bound state. These findings suggest that a high-affinity binding signature does not require that the parvalbumin apo- and Ca^{2+}-bound conformations be indistinguishable, as we have recently proposed. They also suggest that it is possible to engineer a Ca^{2+}-dependent conformational change into a high-affinity EF-hand protein, furnishing a mechanism by which the protein could play a reverse Ca^{2+} sensor role.

EF-hand proteins (*1*,*2*) participate broadly in eukaryotic Ca^{2+}-dependent signal transduction pathways (*3*−*5*). For example, the human genome harbors 242 family members (*6*). Many of these function explicitly as regulatory proteins, binding to select effector proteins and modulating their activities. Others serve as mobile intracellular Ca^{2+} buffers, influencing the amplitude and duration of Ca^{2+} signals. The EF-hand family is named for its hallmark Ca^{2+}-binding motif; i.e., the spatial arrangement of its central binding loop and flanking helices can be mimicked with the fingers of the right hand (*7*,*8*).

The ligands to the metal ion are positioned at the approximate vertices of an octahedron and, accordingly, are referenced by the axes of a Cartesian coordinate system. EF-hand motifs are generally classified as Ca^{2+}/Mg^{2+} sites or Ca^{2+}-specific sites. The former, also known as high-affinity or mixed sites, exhibit high affinity for Ca^{2+} ($K_{Ca} > 10^7$ M^{-1}) and physiologically relevant affinity for Mg^{2+} ($K_{Mg} > 10^4$ M^{-1}). The latter, also known as low-affinity sites, exhibit moderate affinity for Ca^{2+} (10^5−10^6 M^{-1}) and low affinity for Mg^{2+} ($K_{Mg} < 10^3$ M^{-1}).

Parvalbumins are small EF-hand proteins expressed by vertebrates (*7*,*9*,*10*). The family includes α- and *β*-sublineages (*11*,*12*), which can be distinguished on the basis of isoelectric point (α > 5) and several lineage-specific sequence assignments. The parvalbumin (PV) tertiary structure consists of six helical segments (A−F) organized into two domains: the N-terminal AB domain (residues 1−38) and the CD-EF metal ion-binding domain. The two Ca^{2+}-binding sites are called the CD and EF sites, in reference to the helices flanking the metal ion-binding loops. The CD site[1] includes residues 41−70; the EF site includes residue 80 through the C-terminus.

*To whom correspondence should be addressed. Tel: 573-882-7485. Fax: 573-884-4812. E-mail: henzlm@missouri.edu.

†This work was supported by NSF Award MCB0543476 (to M.T.H.).

[1]Abbreviations: ANS, 1-anilinonaphthalene-8-sulfonic acid; CD, circular dichroism; CaM, calmodulin; CD site, parvalbumin metal ion-binding site flanked by the C and D helical segments; DMPC, dimyristoylphosphatidylcholine; DPPC, dipalmitoylphosphatidylcholine; DSC, differential scanning calorimetry; DSPC, distearoylphosphatidylcholine; EDTA, ethylenediaminetetraacetic acid; EF site, parvalbumin metal ion-binding site flanked by the E and F helical segments; EGTA, ethylene glycol bis(*β*-aminoethyl ether)-*N*,*N*,*N*′,*N*′-tetraacetic acid; HBS, Hepes-buffered saline; Hepes, 4-(2-hydroxyethyl)-1-piperazineethanesulfonic acid; IPTG, isopropyl *β*-D-thiogalactopyranoside; ITC, isothermal titration calorimetry; PBS, phosphate-buffered saline; P_i, phosphate; THP, tris(hydroxypropyl)phosphine.

 Published on Web 3/16/2009

Avian thymic hormone (ATH) is one of two β-PV isoforms expressed in chicken. The other is known as CPV3, short for chicken parvalbumin 3 (*13*). Although ATH was named for its capacity to stimulate avian T-cell differentiation and proliferation (*14*,*15*), the sequence of the protein is unmistakably that of a β-parvalbumin (*16*,*17*). The metal ion-binding properties of ATH have been examined by $^{45}Ca^{2+}$ flow dialysis (*18*) and isothermal titration calorimetry (ITC) (*19*). The Ca^{2+}-binding constants are 2.4×10^8 and 1.0×10^8 M^{-1}; the corresponding Mg^{2+} constants are 2.2×10^4 and 1.2×10^4 M^{-1}. Both sites are unquestionably high-affinity, or Ca^{2+}/Mg^{2+}, sites. However, spectroscopic and hydrodynamic data described below suggest that the conformations of apo- and Mg^{2+}-bound ATH differ significantly from that of the Ca^{2+}-bound state.

MATERIALS AND METHODS

Reagents and Chemicals. NaCl, Hepes, $CaCl_2 \cdot H_2O$, $MgCl_2 \cdot 2H_2O$, EGTA, $Na_2EDTA \cdot 2H_2O$, NaH_2PO_4, lysozyme, and Spectrapor 1 dialysis tubing (MWCO 6000−8000) were purchased from Fisher Scientific Co. LB agar, LB broth, and ampicillin were obtained from Research Products International. IPTG was purchased from Gold Biotechnology. DEAE-Sepharose, Sephadex G-75, THP, and ANS were obtained from Sigma-Aldrich Co. Melittin (>98% purity) was also purchased from Sigma-Aldrich and used without further purification. Its concentration was determined spectrophotometrically, employing a molar absorptivity of 5570 M^{-1} cm^{-1} (*20*).

Protein Isolation. The codon-optimized sequence of ATH (purchased from Genscript Corp.) was cloned into pET11a (Novagen). *Escherichia coli* BL21(DE3), harboring the ATH-pET11 vector, were cultured at 37 °C in LB broth containing ampicillin. Sixteen hours after induction with IPTG, the cell paste was collected by centrifugation. The bacteria were disrupted with a French pressure cell following treatment with lysozyme, and the clarified lysate was subjected to anion-exchange chromatography on DEAE-agarose and gel-filtration chromatography on Sephadex G-75. The purity of the resulting material exceeded 98%. The isolation of ATH has been described in detail previously (*19*). ATH concentrations were determined spectroscopically, employing a molar absorptivity at 274 nm of 1670 M^{-1} cm^{-1}. The procedures employed for purification of rat α-PV, rat β-PV, and CPV3 are described elsewhere (*19*,*21*,*22*).

Prior to experimentation, Ca^{2+} was removed from the proteins by passage over EDTA−agarose (*23*), as described previously (*24*) . The residual Ca^{2+} content was less than 0.02 equiv in each case.

Mouse calmodulin (CaM) was used as a positive control in assays designed to detect formation of a protein−melittin complex. The coding sequence, in pBluescript II SK (Stratagene), was expressed at 37 °C in *E. coli* DH5α. The protein was isolated by minor modification of the method described above for purification of ATH.

Spectroscopy. Circular dichroism (CD) data were collected at 25 °C with an Aviv 62DS spectrometer. To compare the spectra of apo-, Ca^{2+}-bound, and Mg^{2+}-bound ATH, the Ca^{2+}-free protein was diluted to 50 μM in Hepes-buffered saline (HBS) containing 1.0 mM EDTA, 200 μM Ca^{2+}, or 2.0 mM Mg^{2+} and 1.0 mM EGTA. EGTA was included in the Mg^{2+}-containing buffer solution to ensure that contaminating Ca^{2+} would not be bound by the protein. Data were collected at 1 nm intervals between 250 and 200 nm, using a 0.10 cm quartz cuvette, averaging each data point for 5 s.

The ANS emission spectrum was examined in the absence and presence of added protein (ATH, CPV3, rat α-PV, or rat β-PV), using an SLM-Aminco 8100 fluorometer, modified for photon counting (by ISS Inc., Champagne, IL). Employing an excitation wavelength of 365 nm, emission data were collected at 1 nm intervals between 380 and 600 nm, averaging for 1 s at each point. The bandpass was set at 4 nm for both excitation and emission channels. Except for dividing the emission signal by the reference channel output, the spectra are uncorrected.

A nominal 1.0 mM ANS solution in HBS was standardized spectrophotometrically, employing an extinction coefficient of 4950 M^{-1} cm^{-1} (*25*). The stock solution was subsequently diluted to 10 μM in HBS containing either 200 μM Ca^{2+}, 5.0 mM EDTA, or 2.0 mM Mg^{2+} and 1.0 mM EGTA. After the spectrum of the ANS alone was collected, aliquots of Ca^{2+}-free protein were added to the ANS solution to yield nominal concentrations of 25, 50, 75, and 100 μM protein. All data were collected at 25 °C using a 1.0 cm quartz cuvette.

Sedimentation Velocity. Following dialysis against the appropriate buffer, ATH (6.5 mg/mL) and buffer were loaded into the sample and reference chambers, respectively, of a charcoal-Epon dual-sector centerpiece. To study the Ca^{2+}-free form of the protein, the ATH was dialyzed extensively at 4 °C against HBS containing 5.0 mM EDTA; the Mg^{2+}-bound form was similarly obtained by dialysis against HBS containing 2.0 mM Mg^{2+} and 1.0 mM EGTA; and the Ca^{2+}-bound protein was obtained by dialysis against HBS containing 200 μM Ca^{2+}. In each case, the buffer also contained 1.0 mM THP to prevent oxidation of Cys-18. After the rotor had equilibrated at 20 °C for 2 h under vacuum, the centrifuge was accelerated to 45000 rpm. Data acquisition was initiated immediately upon reaching speed and continued until 150 radial absorbance scans (at 274 nm) had been collected. The continuous $c(s)$ distributions were obtained with Sedfit v.9.4 (*26*). Monte Carlo analysis was used to estimate the uncertainties in the reported maxima, employing 500 synthetic data sets. Solution viscosity, required for estimation of the axial ratio from the sedimentation coefficient, was measured at 20 °C using an Ostwald viscometer.

Sedimentation Equilibrium. Following extensive dialysis against HBS containing 5.0 mM EDTA and 1.0 mM THP, a mixture of ATH and melittin (each present at 30 μM) was sedimented to equilibrium at 20 °C, employing rotor speeds of 20000, 30000, and 40000 rpm. A comparable experiment was also performed with calmodulin, following dialysis of the CaM−melittin sample against HBS containing 100 μM Ca^{2+}. Whereas ATH and CaM are both devoid of tryptophan, the 26-residue sequence of melittin harbors a tryptophan at position 19. Thus, it is possible to selectively monitor the radial distribution of

melittin by collecting absorbance data at 295 nm. The resulting data were fit to an ideal single-species model:

$$a = a_o \exp\left[\frac{M\omega^2(1-\bar{v}\rho)}{2RT}(r^2 - r_o{}^2)\right] + \text{bl} \qquad (1)$$

where a is the absorbance at radial position r, a_o the absorbance at an arbitrary reference position r_o, M the molecular weight, ω the angular velocity, $\bar{v}$ the partial specific volume, ρ the solution density, R the gas constant, and T the absolute temperature. bl is a baseline offset to correct for any optical mismatch between the sample and solvent sectors. The partial specific volumes of melittin, ATH, and CaM were assumed to be 0.73 cm^3/g, and the solvent density, measured with an Anton-Paar DMA 5000 densimeter, was found to be 1.0066 g/cm^3.

Differential Scanning Calorimetry. DSC was performed in a Nano-DSC (Calorimetry Sciences Corp.), equipped with cylindrical hastalloy cells having nominal volumes of 0.32 mL. Temperature calibration was confirmed with DMPC, DPPC, and DSPC. The accuracy of the differential power measurements was confirmed with internally generated electrical calibration pulses.

Samples of ATH were dialyzed extensively against 0.15 M NaCl, 0.01 M NaP_i, 0.005 M EDTA, pH 7.4 (PBS/EDTA), and 0.001 M THP which then served as the reference. Sample and reference solutions were degassed briefly under vacuum prior to loading. A scan rate of 60° per hour was employed for all experiments. ATH exhibits an endotherm on rescan, indicating that the thermal denaturation is reversible. A baseline scan, obtained with sample and reference cells filled with buffer, was subtracted from the protein data prior to analysis. Data collected at several protein concentrations were subjected to global nonlinear least-squares analysis to extract estimates of T_m, ΔH_{vH}, ΔH_{cal}, and ΔC_p, as described elsewhere (*27*). The conformational stability at 25 °C was estimated using the integrated Gibbs−Helmholtz equation:

$$\Delta G(T) = \Delta H_{vH}(T_m)\left(1 - \frac{T}{T_m}\right) + \Delta C_p\left[(T - T_m) - T \ln \frac{T}{T_m}\right] \qquad (2)$$

Isothermal Titration Calorimetry. Aliquots (14 μL) of 100 μM Ca^{2+}-free ATH were added to 10 μM melittin in HBS, containing 5 mM EDTA, at 25 °C, in a MicroCal VP-ITC. For comparison, additions of ATH were also made to buffer alone. A comparable titration was also conducted with calmodulin, making additions (10 μL) of the Ca^{2+}-bound protein (80 μM) to a 6.0 μM solution of melittin in HBS containing 100 μM Ca^{2+}. The integrated ITC data were analyzed with the software supplied with the instrument.

RESULTS

Far-UV Circular Dichroism. With pronounced minima at 222 and 208 nm, the far-UV CD spectrum of ATH is characteristic of a protein possessing high helical content (Figure 1). Although ligation state does not have a major impact on the appearance of the spectrum, Ca^{2+} binding promotes a small, but reproducible, increase in ellipticity (○). Interestingly, Mg^{2+} binding does not produce a comparable change. The spectra obtained in the presence of Mg^{2+} (□) and excess EDTA (△) are nearly superimposable.

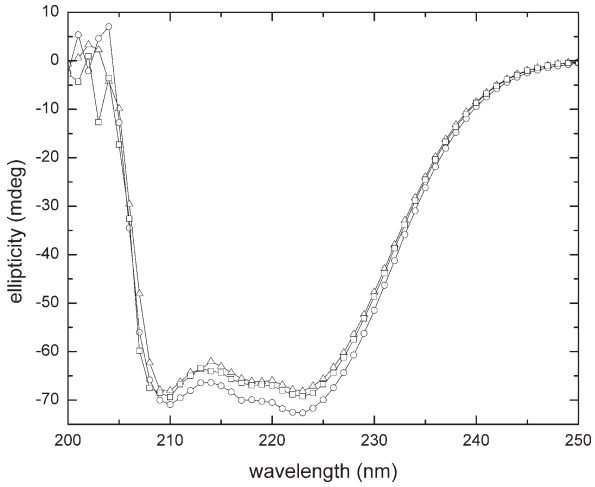

FIGURE 1: Influence of ligation state on the far-UV circular dichroism spectrum of ATH. The far-UV CD spectrum of ATH was collected in Hepes-buffered saline containing either 0.2 mM Ca^{2+} (○), 2.0 mM Mg^{2+} and 1.0 mM EGTA (□), or 5.0 mM EDTA (△).

ANS Fluorescence. The suggestion that Ca^{2+} binding provokes a perceptible conformational change is supported by fluorescence measurements on 1-anilinonaphthalene-8-sulfonic acid (ANS). The quantum yield of ANS is exquisitely sensitive to solvent polarity, and the dye is frequently employed as a probe of solvent-accessible apolar surface area (*28*). In HBS, the emission from ANS exhibits a relatively sharp feature at 498 nm superimposed on a broad spectrum having a maximum at 530 nm. Addition of ATH to the ANS solution in the presence of excess Ca^{2+} produces a modest increase in fluorescence at 498 nm (Figure 2A), indicating that the Ca^{2+}-bound protein is largely devoid of solvent-accessible apolar surface.

By contrast, if Ca^{2+}-free ATH is added to the ANS in the presence of excess EDTA, there is a substantial increase in emission intensity and an accompanying shift in the emission maximum to 475 nm (Figure 2B), over the same range of protein concentration. This observation suggests that the conformation of the Ca^{2+}-free protein differs perceptibly from that of the Ca^{2+}-bound state, exposing a significant area of apolar surface for interaction with the dye. If the same experiment is performed in the presence of Mg^{2+}, the behavior closely resembles that observed for the Ca^{2+}-free protein (Figure 2C). The ANS emission increases markedly and shifts to lower wavelength.

For comparison, analyses were performed with three other parvalbumin isoforms: rat α-PV (Figure 3), CPV3 (Figure 4), and rat β-PV (Figure 5). Addition of rat α-PV causes no significant increase in ANS emission, either in the Ca^{2+}-bound (Figure 3A) or Ca^{2+}-free state (Figure 3B). Although Ca^{2+}-bound CPV3 has no impact on the dye fluorescence (Figure 4A), addition of the Ca^{2+}-free protein affords a minor increase in signal intensity at 498 nm (Figure 4B).

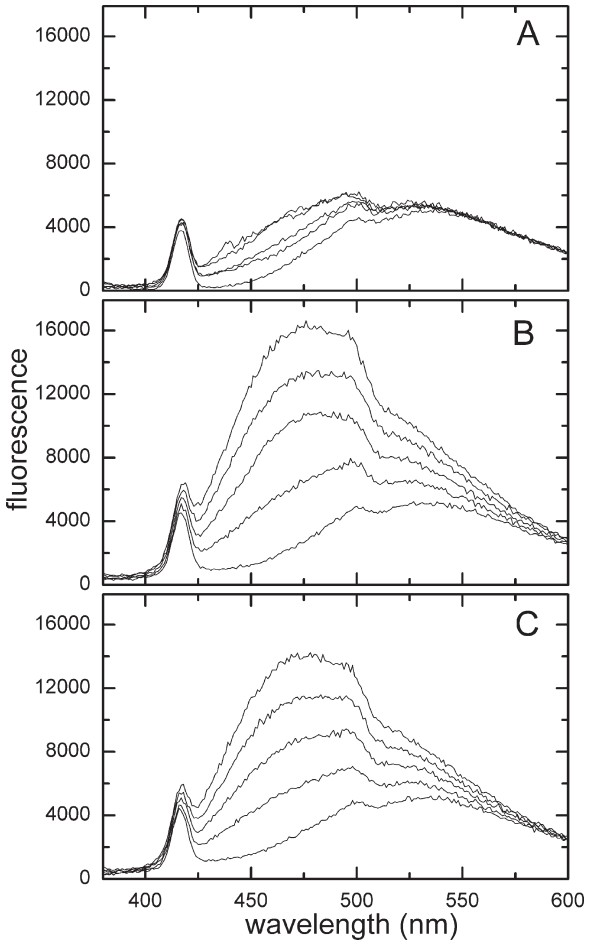

FIGURE 2: Influence of ATH on ANS fluorescence emission. Aliquots of Ca^{2+}-free ATH were added to 10 μM ANS (bottom trace in each panel) in Hepes-buffered saline containing 1.0 mM Ca^{2+} (A), 5.0 mM EDTA (B), or 2.0 mM Mg^{2+} and 1.0 mM EGTA (C). Nominal final protein concentrations were 25, 50, 75, and 100 μM. The feature at 417 nm is due to Raman scattering from the solvent.

The effect of rat β-PV on ANS emission is interesting. Perceptible increases in signal intensity are observed for all three ligation states. As with ATH, addition of the Ca^{2+}-free protein has the greatest impact. However, the blue shift in the emission maximum is less pronounced. Significantly, whereas the behavior observed with ATH in the presence of Mg^{2+} closely resembles that observed for the apoprotein, the behavior observed with rat β-PV in the presence of Mg^{2+} is indistinguishable from that observed in the presence of saturating Ca^{2+}.

The ANS fluorescence data for all four parvalbumin isoforms are summarized in Figure 6. The emission signal, normalized to the signal intensity measured in the absence of added protein, is plotted vs the concentration of added protein. Data for the apo, Mg^{2+}-bound, and Ca^{2+}-bound forms of the protein are represented by circles (○), squares (□), and triangles (△), respectively.

Sedimentation Velocity. CD and ANS fluorescence measurements suggested that the tertiary structures of apo- and Mg^{2+}-bound ATH differ perceptibly from that of the Ca^{2+}-bound form. Sedimentation velocity analyses were performed to determine whether the translational frictional coefficient is a function of ligation state. Samples of the protein were sedimented at 45000 rpm, at

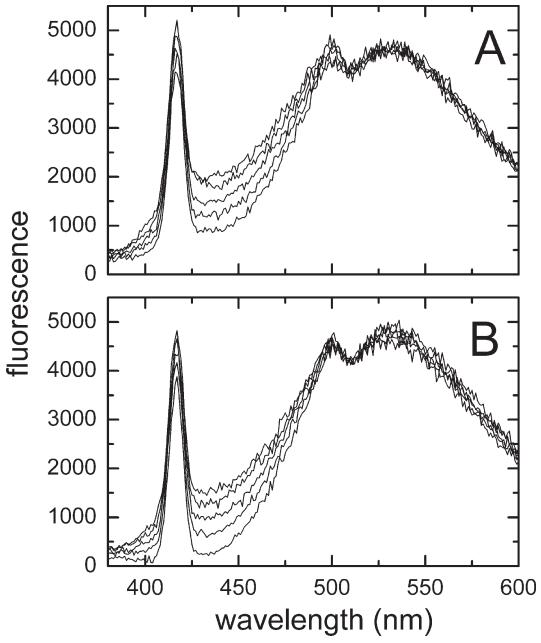

FIGURE 3: Impact of rat α-PV on ANS emission. ANS fluorescence analysis. Aliquots of Ca^{2+}-free rat α-PV were added to 10 μM ANS (bottom trace in each panel) in Hepes-buffered saline, pH 7.4, containing either 1.0 mM Ca^{2+} (A) or 5.0 mM EDTA (B). Nominal final protein concentrations were 25, 50, 75, and 100 μM.

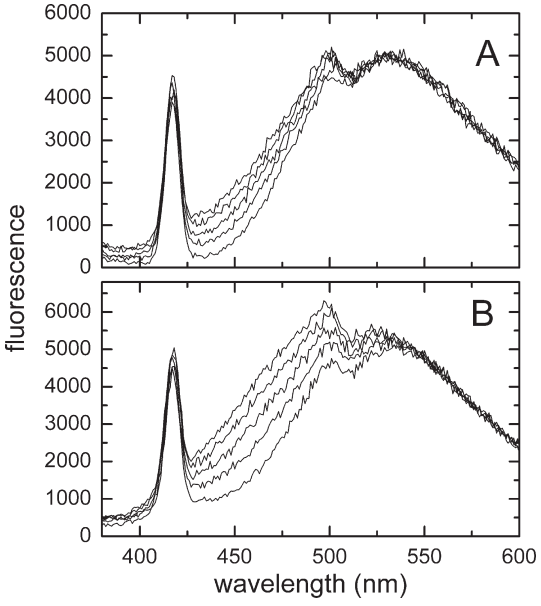

FIGURE 4: Impact of CPV3 on ANS emission. Aliquots of Ca^{2+}-free CPV3 were added to 10 μM ANS (bottom trace in each panel) in Hepes-buffered saline, pH 7.4, containing either 1.0 mM Ca^{2+} (A) or 5.0 mM EDTA (B). Nominal final protein concentrations were 25, 50, 75, and 100 μM.

20 °C, in either the presence of Ca^{2+}, Mg^{2+}/EGTA, or EDTA. A total of 150 scans were collected in each case. The entire data set was analyzed with Sedfit to extract estimates for the apparent sedimentation coefficient.

The resulting $c(s)$ distributions are displayed in Figure 7, and the maxima are listed in Table 1. Whereas the maximum in the distribution for the Ca^{2+}-bound protein occurs at 1.45 ± 0.01 S, the peak in the apo-ATH distribution occurs at 1.35 ± 0.01 S. In the presence of Mg^{2+}/EGTA, the maximum is observed at 1.39 ± 0.01 S.

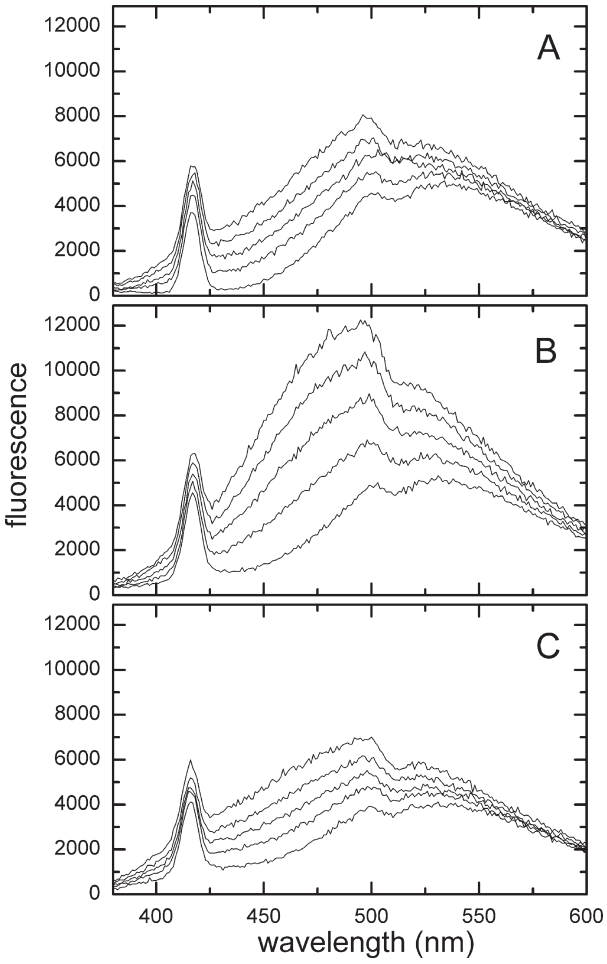

FIGURE 5: Impact of rat β-PV on ANS emission. Aliquots of Ca^{2+}-free rat β-PV were added to 10 μM ANS (bottom trace in each panel) in Hepes-buffered saline, pH 7.4, containing 1.0 mM Ca^{2+} (A), 5.0 mM EDTA (B), or 2.0 mM Mg^{2+} and 1.0 mM EGTA (C). Nominal final protein concentrations were 25, 50, 75, and 100 μM.

Differential Scanning Calorimetry. The stability of Ca^{2+}-free ATH was examined by scanning calorimetry in PBS/EDTA. Figure 8 presents data collected at protein concentrations of 1.9, 3.8, and 5.8 mg/mL. The data were subjected to global least-squares analysis to extract estimates for the melting temperature (T_m), the van't Hoff enthalpy (ΔH_{vH}), the calorimetric enthalpy (ΔH_{cal}), and the change in heat capacity upon denaturation (ΔC_p). The optimal values for these parameters, and their associated experimental uncertainties, are listed in Table 2. Whereas ΔH_{vH} describes the temperature dependence of the equilibrium constant for unfolding, ΔH_{cal} is estimated from the area under the heat capacity curve. Their ratio is indicative of the cooperativity of the unfolding transition. A perfect two-state transition will yield a $\Delta H_{vH}/\Delta H_{cal}$ ratio of 1.0. The value obtained for the thermal denaturation of ATH, 0.90, implies that there is some population of partially unfolded intermediates. However, greater deviations from unity have been observed for site-specific variants of rat β-PV (*27*,*29*). Substituting the observed values for T_m, ΔH_{vH}, and ΔC_p into eq 2 yields an estimate for the conformational stability of the apoprotein at 25 °C of 3.1 kcal/mol.

ATH Does Not Bind Melittin. Two decades ago, Permyakov et al. (*30*) observed an interaction between melittin, an amphipathic peptide present in bee venom, and Ca^{2+}-free parvalbumin isoforms from pike. Accordingly, we tested ATH for the ability to bind the peptide. In ITC experiments, the heat effects that accompany addition of ATH to a solution of melittin at 25 °C are small and comparable to those obtained by addition of ATH to buffer alone (Figure 9A). By contrast, addition of calmodulin, known to associate with melittin in the presence of Ca^{2+} (*31*), produces substantial endothermic heat effects. Analysis of the integrated data (Figure 9B), collected in the presence of 100 μM Ca^{2+}, yielded estimates for the apparent binding constant and binding enthalpy of $(3.4 \pm 1.4) \times 10^8$ M^{-1} and 9.7 ± 0.1 kcal/mol, respectively.

To confirm the absence of an interaction between melittin and ATH, we subjected the peptide to sedimentation equilibrium in the presence of the protein. Because ATH lacks tryptophan, the absorbance at 295 nm can be used to selectively monitor the radial distribution of melittin. The optimal least-squares fit to data gathered at 20000, 30000, and 40000 rpm (Figure 9C) yields a molecular weight estimate of 2900 ± 1180, in good agreement with the sequence-derived monomeric molecular weight of the peptide, 2850. By contrast, when the experiment is performed in the presence of Ca^{2+}-bound calmodulin (Figure 9D), likewise devoid of tryptophan, the apparent molecular weight increases to 19100 ± 300. This latter value is approximately equal to the combined molecular weights of melittin (2850) and calmodulin (16840), consistent with formation of a high-affinity CaM−melittin complex.

DISCUSSION

EF-hand sensor proteins, i.e., those with explicit Ca^{2+}-dependent regulatory activity, often expose apolar surface area upon binding Ca^{2+}, presumably for interaction with effector molecules. This behavior is widely viewed as *de facto* evidence for a regulatory function. Thus, the pollen-specific EF-hand proteins known as polcalcins are believed to regulate pollen-tube growth, although the putative biological target remains unidentified.

In fact, the initial ANS fluorescence measurements on ATH were made while characterizing Phl p 7, a polcalcin from timothy grass. Addition of Ca^{2+}-loaded Phl p 7 to a solution of ANS produces a substantial increase in the quantum yield of the dye. By contrast, the apo and Mg^{2+}-bound forms are without effect (*32*). ATH was to serve as an example of a protein with no significant impact on ANS emission in either apo or divalent ion-bound forms.

Contrary to expectation, although Ca^{2+}-bound ATH is without effect, the apoprotein provokes a major increase in ANS emission and a pronounced blue shift. Significantly, the Mg^{2+}-bound protein has a comparable impact. The ANS fluorescence data imply that the apo and Mg^{2+}-bound forms of ATH present an apolar surface for interaction with the dye. The conclusion that ligation state significantly influences conformation is supported by far-UV circular dichroism measurements. Whereas the CD spectra of the Mg^{2+}-bound and apo forms of the protein are virtually superimposable, the

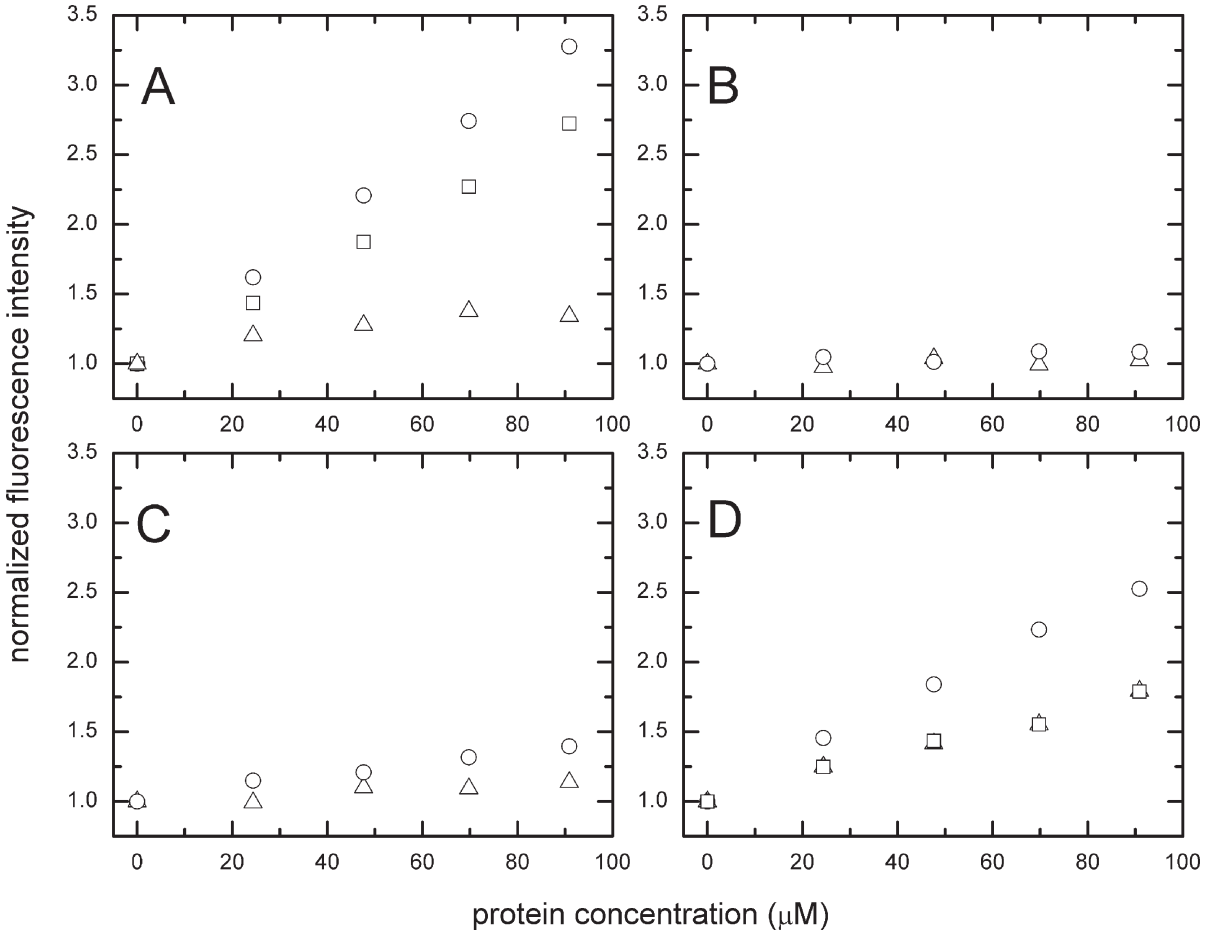

FIGURE 6: Summary of ANS fluorescence data. Normalized ANS emission is plotted as a function of added protein concentration for ATH (A), rat α-PV (B), CPV3 (C), and rat β-PV (D). Apoprotein data, collected in the presence of excess EDTA, are indicated with circles (○). Mg^{2+}-bound protein data, collected in the presence of Mg/EGTA, are indicated with squares (□). Ca^{2+}-bound protein data, collected in the presence of saturating Ca^{2+}, are indicated with triangles (△). All protein concentrations have been corrected for dilution. The normalized emission values were obtained by dividing the signal intensity, at the appropriate wavelength, by the signal intensity observed in the absence of added protein.

spectrum of the Ca^{2+}-bound protein exhibits perceptibly greater ellipticity at 222 and 208 nm.

The impact of ATH on ANS fluorescence is not general. Rat α-PV has no effect on ANS emission in either the apo- or Ca^{2+}-bound forms. Much the same can be said for CPV3, although a very minor increase in ANS fluorescence is observed upon addition of the Ca^{2+}-free protein.

Addition of Ca^{2+}-free rat β-PV causes a substantial increase in ANS emission, but the blue shift is less pronounced. Unlike ATH, there is also a perceptible increase in ANS emission in the presence of saturating Ca^{2+}. Moreover, the behavior observed in the presence of Mg^{2+} mimics the Ca^{2+}-bound protein, rather than the apoprotein.

Permyakov recently reported that the pike pI 4.2 and pI 5.0 parvalbumin isoforms are disordered in the absence of divalent ions (*33*). However, the apo and Mg^{2+}-bound forms of ATH do not appear to be disordered. The CD spectra indicate that both possess a degree of helical structure comparable to that in the Ca^{2+}-bound protein. Additionally, the cooperative thermal unfolding event observed by DSC indicates that the apoprotein possesses a well-defined tertiary structure.

Sedimentation velocity measurements were performed on apo-, Mg^{2+}-bound, and Ca^{2+}-bound ATH to further explore conformational differences. The apparent translational frictional coefficient f for a sedimenting particle is related to the observed sedimentation coefficient s by the equation:

$$f = \frac{M(1-\bar{v}\rho)}{Ns} \quad (3)$$

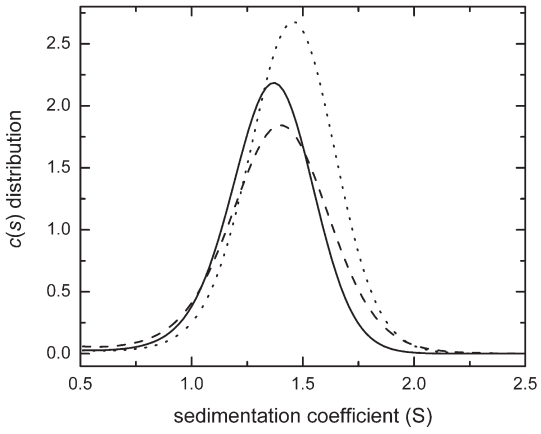

FIGURE 7: Impact of ligation state on the sedimentation coefficient of ATH. Samples of ATH (6.7 mg/mL) were centrifuged at 20 °C and 45000 rpm in Hepes-buffered saline containing 5.0 mM EDTA (solid line), 2 mM Mg^{2+} and 1.0 mM EGTA (dashed line), or 1.0 mM Ca^{2+} (dotted line). The sedimentation coefficient distribution, $c(s)$, was evaluated using Sedfit.

Table 1: Hydrodynamic Behavior of ATH in the Apo, Mg^{2+}-Bound, and Ca^{2+}-Bound Forms

			predicted axial ratio[a]		
ligation state	s (S)	f	$\delta = 0.35$	$\delta = 0.40$	$\delta = 0.45$
apo	1.35 ± 0.01	$3.82\,(0.03) \times 10^{-8}$	2.90 (3.14)	2.71 (2.95)	2.53 (2.77)
Mg^{2+}-bound	1.39 ± 0.01	$3.71\,(0.03) \times 10^{-8}$	2.44 (2.68)	2.25 (2.50)	2.07 (2.31)
Ca^{2+}-bound	1.45 ± 0.01	$3.56\,(0.03) \times 10^{-8}$	1.76 (2.02)	1.53 (1.82)	1.25 (1.61)

[a] The first number was obtained using the estimate of Stokes's radius calculated with eq 8; the number in parentheses was obtained using the Stokes's radius calculated with eq 5.

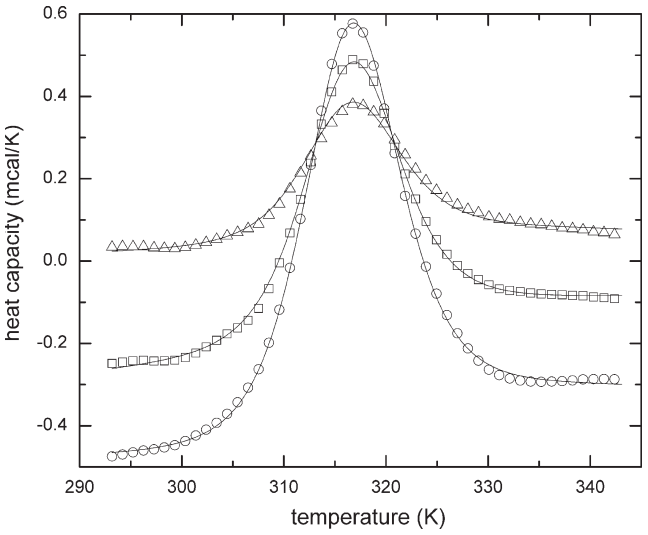

FIGURE 8: Thermal stability of Ca^{2+}-free ATH. Following dialysis against PBS, pH 7.4, containing 5.0 mM EDTA, samples of ATH were examined by DSC. The sample concentrations were 1.9 (△), 3.8 (□), and 5.8 (○) mg/mL. For clarity, only subsets of the data points are presented. The solid lines represent the optimal least-squares fit to a two-state unfolding model.

where M is the particle molecular weight, $\bar{v}$ the partial specific volume, ρ the solution density, and N Avogadro's number. The predicted frictional coefficient for an unhydrated, spherical protein is given by Stokes's law:

$$f_o = 6\pi\eta r_o \tag{4}$$

where η is the solvent viscosity, determined to be 0.0109 P, and r_o is the protein radius:

$$r_o = (3M\bar{v}/4\pi N)^{1/3} \tag{5}$$

The ratio f/f_o, which depends on both shape and the extent of hydration, can be expressed as the product of shape and hydration terms:

$$f/f_o = (f/f_{sp})(f_{sp}/f_o) \tag{6}$$

In eq 6, f_{sp} is the frictional coefficient for a spherical molecule of mass M having some specified hydration. Thus, (f_{sp}/f_o) compares the frictional coefficients for hydrated and unhydrated spheres of mass M and is equal to $(1 + \delta/\rho)^{1/3}$, where δ is the extent of hydration. Typical values of δ for proteins fall in the range between 0.3 and 0.5. Equations 3−6 are described in greater detail in ref *34*.

The f/f_{sp} term in eq 6 is a shape factor. For a prolate ellipsoid with semimajor axis a and semiminor axis b, it is related to the axial ratio, $P = a/b$, by the equation (*35*):

$$f/f_{sp} = \frac{P^{-1/3}(P^2 - 1)^{1/2}}{\ln\left[P + (P^2 - 1)^{1/2}\right]} \tag{7}$$

Assuming a value of 0.4 g of H_2O/g of ATH, f_{sp}/f_o is equal to 1.119. Division of f/f_o by this quantity yields f/f_{sp}. The resulting value can be substituted into eq 7, which is then solved numerically for P. Predicted axial ratio values for the three ligation states of ATH are listed in Table 2. For reference, the axial ratio estimated from the crystal structure of Ca^{2+}-bound carp parvalbumin is approximately 1.2 (*7*). Because the choice of $\delta = 0.40$ is somewhat arbitrary, axial ratios are tabulated for δ values of 0.35 and 0.45 as well. Additionally, it has been argued that application of eq 5 leads to an underestimation of r_o and a resulting overestimation of the axial ratio. Teller (*36*) suggested this alternative empirical relationship for calculating the protein radius (r_p):

$$r_p = 6.72 \times 10^{-9}\ M^{1/3} \tag{8}$$

Thus, axial ratios have been calculated for both r_o and r_p. Although the exact values are sensitive to the choice of r and δ, it is apparent that the axial ratio of the Ca^{2+}-free protein is significantly larger than that of the Ca^{2+}-bound protein. An intermediate value is obtained for the Mg^{2+}-bound protein. Presumably, the structuring of the CD and EF binding loops that accompanies their occupation by Mg^{2+} causes some contraction along the semimajor axis.

Recall that the PV molecule consists of two domains, the N-terminal AB domain and the CD-EF domain. There are currently just two apoparvalbumin structures in the database, those of the rat α- and β-isoforms (*37*,*38*). Although the AB and CD-EF domains remain tightly associated in both structures, removal of Ca^{2+} from rat β-PV evidently alters their relative orientation. Conceivably, the extent of AB/CD-EF association in the absence of Ca^{2+} could be isoform-dependent. The hydrodynamic analysis discussed above suggests that the apo and Mg^{2+}-bound proteins show greater departures from spherical symmetry than the Ca^{2+}-bound protein. This finding is consistent with incomplete association between the AB and CD-EF domains.

The DSC analysis lends supports to this idea. The data can be satisfactorily accommodated by a two-state model, suggesting that the Ca^{2+}-free protein unfolds cooperatively. The optimal value of ΔC_p, 1.03 kcal mol^{-1} K^{-1}, is

Table 2: Results of DSC Analysis[a]

protein	T_m (K)	ΔH_{cal} (kcal mol^{-1})	ΔH_{vH} (kcal mol^{-1})	$\Delta H_{vH}(60)$ (kcal mol^{-1})	ΔC_p (kcal mol^{-1} K^{-1})	ΔASA_{ap} (Å^2)	ΔASA_p (Å^2)
ATH	316.1 (315.9, 316.2)	72.4 (71.9, 73.5)	64.8 (64.0, 65.0)	82.1	1.03 (1.02, 1.18)	4500	3830
rat β-PV[b]	322.4 (322.3, 322.6)	72.9 (72.5, 73.1)	67.9 (67.7, 68.2)	84.9	1.60 (1.57, 1.63)	6060	4330

[a] Numbers in parentheses represent the 90% confidence intervals. [b] From Henzl et al. (*27*).

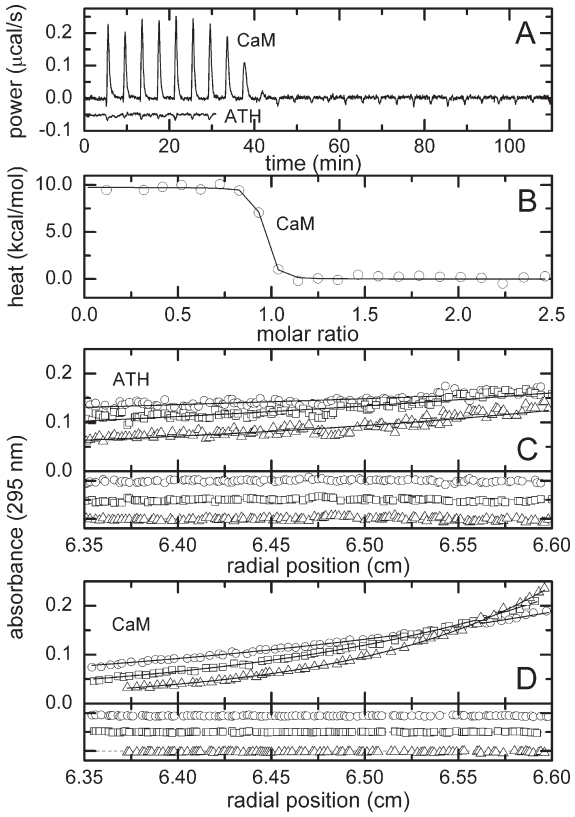

FIGURE 9: Melittin does not associate with apo-ATH. (A) Raw ITC data are displayed for the addition of either apo-ATH or Ca^{2+}-bound CaM (positive control) to a solution of melittin. The experiments were conducted at 25 °C, in Hepes-buffered saline, pH 7.4, containing either 5.0 mM EDTA or 100 μM Ca^{2+}, respectively. Data are offset for clarity. (B) Integrated ITC data for the titration with CaM displayed in panel A. (C) Sedimentation equilibrium analysis of melittin in the presence of apo-ATH. An equimolar mixture of melittin and ATH (each present at 30 μM) was sedimented to equilibrium at 20 °C and rotor speeds of 20000, 30000, and 40000 rpm. The solid line reflects the best least-squares fit to the data. (D) Corresponding data for melittin in the presence of Ca^{2+}-bound CaM. Peptide and protein (each present at 22 μM) were sedimented at 20 °C and rotor speeds of 20000, 30000, and 40000 rpm.

significantly lower than that determined for Ca^{2+}-free rat β-PV, 1.60 kcal mol^{-1} K^{-1}. Applying the scaling factors reported by Xie and Freire (*39*), the values for the change in heat capacity and the extrapolated enthalpy change at 60 °C can be related to the associated changes in surface area through these equations:

$$\Delta C_p = 0.45\Delta ASA_{ap} - 0.26\Delta ASA_p \quad (9)$$

$$\Delta H(60) = 31.4\Delta ASA_p - 8.44\Delta ASA_{ap} \quad (10)$$

In eqs 9 and 10, $\Delta H(60)$ and ΔC_p are expressed in units of cal mol^{-1} and cal mol^{-1} K^{-1}, respectively, and ΔASA_{ap} and ΔASA_p represent the changes in solvent-accessible apolar and polar surface area, respectively, in Å^2. Substituting the values of ΔC_p and $\Delta H(60)$ for Ca^{2+}-free ATH into the equations and solving for ΔASA_{ap} and ΔASA_p afford values of 4500 and 3830 Å^2, respectively. Corresponding values of 6060 and 4330 Å^2 are obtained for the rat β-isoform. The implication is that, relative to rat β-PV, thermal denaturation of apo-ATH is accompanied by exposure of less surface area, particularly apolar surface area. This conclusion is consistent with the idea that the hydrophobic aspects of the AB and CD-EF domains are solvent accessible in the apoprotein, and in the Mg^{2+}-bound protein by extension, due to incomplete association of the two domains.

The notion that the Mg^{2+}-bound protein more closely resembles the apoprotein than the Ca^{2+}-bound form is perhaps the most interesting suggestion to emerge from this study. The CD and EF sites in ATH both bind Ca^{2+} and Mg^{2+} with high affinity. To our knowledge, ATH is the first high-affinity parvalbumin observed to display a Ca^{2+}-specific conformational change. Hutnik et al. (*40*) previously presented spectroscopic evidence for a Ca^{2+}-specific conformational change in cod β-parvalbumin. However, the binding sites in that protein are distinctly nonequivalent. The fluorescence data of Hutnik et al. indicate that the sites titrate sequentially. Moreover, the Ca^{2+}-binding constants for the CD and EF sites in the virtually identical protein from whiting differ by more than 2 orders of magnitude (*41*).

A priori, there is no reason that the binding of Mg^{2+} and Ca^{2+} should provoke identical conformational changes. The two ions differ in terms of their coordination within the EF-hand site. Whereas the $-z$ glutamyl side chain coordinates Ca^{2+} in a bidentate manner, so that the overall coordination is pentagonal bipyramidal, it functions as a monodentate ligand to Mg^{2+} (*42*). However, in pike pI 4.1 parvalbumin, the structural differences that accompany binding of Mg^{2+} and Ca^{2+} are relatively minor and largely confined to the immediate vicinity of the binding loop (*43*). In ATH, the differences in Ca^{2+} and Mg^{2+} coordination geometry apparently have global structural consequences.

In addition to its endocrine function in the avian immune system, ATH has also been detected in the avian visual system (*44*). Although it has been tacitly assumed that the protein is acting as a Ca^{2+} buffer in this setting, the data presented here suggest an alternative possibility, namely, that ATH might actually be serving as a reverse Ca^{2+} sensor. Under resting state conditions in the cell, with the cytosolic Ca^{2+} level below 100 nM and Mg^{2+} present at millimolar concentrations, the CD and EF sites in ATH would be occupied by Mg^{2+}. The accessibility of apolar surface area in the Mg^{2+}-bound state could

facilitate noncovalent association of ATH with a biological target protein, either to modulate its activity or merely to sequester it. Following receipt of a Ca^{2+} signal, the subsequent rise in intracellular Ca^{2+} would promote Ca^{2+}/Mg^{2+} exchange in the EF-hand motifs and release of the target protein.

The idea that a parvalbumin might function in this capacity was actually suggested 20 years ago. Permyakov et al. reported that the pI 4.2 and 5.0 parvalbumins from pike associated with melittin, a peptide from bee venom, exclusively in the absence of divalent ions (*30*). The site of interaction on the parvalbumin was not determined in that study, and we are unaware of any subsequent work on the system. Nevertheless, it was an interesting observation, which led the authors to propose that a parvalbumin could serve as a reverse sensor. Parenthetically, as described above, we tested apo-ATH for the capacity to bind melittin, using both ITC and analytical ultracentrifugation. Neither technique yielded evidence for an interaction.

On the basis of structural data for the rat α- and *β*-PV isoforms, we have suggested a relationship between Ca^{2+} affinity and the conformational similarity of the apo and Ca^{2+}-loaded forms. The CD site of rat *β*-PV exhibits anomalously low affinity for divalent ions. In that protein, Ca^{2+} binding provokes a substantial conformational rearrangement (*37*), which prompted speculation that the energetic cost of the structural change reduced the net binding free energy. If correct, then Ca^{2+} binding should be accompanied by more muted structural alterations in high-affinity isoforms. That idea was supported by structural data for the Ca^{2+}-free rat α-isoform, which closely resembles the Ca^{2+}-bound protein (*38*). The results described here for ATH suggest that the correlation between binding affinity and the conformational similarity of the Ca^{2+}-free and Ca^{2+}-loaded states is not that straightforward. ATH evidently offers the example of a parvalbumin that retains very high affinity for divalent ions despite dissimilarity of the apo and Ca^{2+}-bound tertiary structures. Clearly, this issue deserves further examination.

CONCLUSIONS

Although both EF-hand motifs in ATH qualify as Ca^{2+}/Mg^{2+}, or high-affinity, sites, the conformations of the Mg^{2+}- and Ca^{2+}-bound forms of the protein differ significantly. Like the apoprotein, the Mg^{2+}-bound protein exposes apolar surface area for interaction with ANS. Far-UV circular dichroism data likewise suggest that the Mg^{2+}-bound form more closely resembles the apoprotein. Sedimentation velocity data suggest that the apo and Mg^{2+}-bound states are less compact than the Ca^{2+}-bound state. These findings challenge the notion that only low-affinity sites can undergo Ca^{2+}-specific conformational changes. Moreover, they raise the possibility that ATH may play a reverse Ca^{2+} sensor role in the avian vision system.

REFERENCES

1. Celio, M. R., Pauls, T., and Schwaller, B. (1996) *Guidebook to the Calcium-Binding Proteins*, Oxford University Press, New York.
2. Kawasaki, H., and Kretsinger, R. H. (1995) Calcium-binding proteins 1: EF-hands. *Protein Profile 2*, 297–490.
3. Berridge, M. J., Bootman, M. D., and Roderick, H. L. (2003) Calcium signalling: Dynamics, homeostasis and remodelling. *Nat. Rev. Mol. Cell Biol. 4*, 517–529.
4. Kahl, C. R., and Means, A. R. (2003) Regulation of cell cycle progression by calcium/calmodulin-dependent pathways. *Endocr. Rev. 24*, 719–736.
5. Carafoli, E., Santella, L., Branca, D., and Brini, M. (2001) Generation, control, and processing of cellular calcium signals. *Crit. Rev. Biochem. Mol. Biol. 36*, 107–260.
6. Lander, E. S., Linton, L. M., Birren, B., Nusbaum, C., Zody, M. C., and Baldwin, J. (2001) Initial sequencing and analysis of the human genome. *Nature (London) 409*, 860–921.
7. Kretsinger, R. H., and Nockolds, C. E. (1973) Carp muscle calcium-binding protein. II. Structure determination and general description. *J. Biol. Chem. 248*, 3313–3326.
8. Kretsinger, R. H. (1980) Structure and evolution of calcium-modulated proteins. *CRC Crit. Rev. Biochem. 8*, 119–174.
9. Heizmann, C. W., and Kagi, U. (1989) Structure and function of parvalbumin. *Adv. Exp. Med. Biol. 255*, 215–222.
10. Pauls, T. L., Cox, J. A., and Berchtold, M. W. (1996) The Ca^{2+}-binding proteins parvalbumin and oncomodulin and their genes: New structural and functional findings. *Biochim. Biophys. Acta 1306*, 39–54.
11. Goodman, M., and Pechere, J. F. (1977) The evolution of muscular parvalbumins investigated by the maximum parsimony method. *J. Mol. Evol. 9*, 131–158.
12. Moncrief, N. D., Kretsinger, R. H., and Goodman, M. (1990) Evolution of EF-hand calcium-modulated proteins. I. Relationships based on amino acid sequences. *J. Mol. Evol. 30*, 522–562.
13. Hapak, R. C., Zhao, H., Boschi, J. M., and Henzl, M. T. (1994) Novel avian thymic parvalbumin displays high degree of sequence homology to oncomodulin. *J. Biol. Chem. 269*, 5288–5296.
14. Murthy, K. K., and Ragland, W. L. (1984) Immunomodulation by thymic hormones: studies with an avian thymic hormone. *Prog. Clin. Biol. Res. 161*, 481–491.
15. Barger, B., Pace, J. L., and Ragland, W. L. (1991) Purification and partial characterization of an avian thymic hormone. *Thymus 17*, 181–197.
16. Brewer, J. M., Wunderlich, J. K., Kim, D. H., Carr, M. Y., Beach, G. G., and Ragland, W. L. (1989) Avian thymic hormone (ATH) is a parvalbumin. *Biochem. Biophys. Res. Commun. 160*, 1155–1161.
17. Brewer, J. M., Wunderlich, J. K., and Ragland, W. L. (1990) The amino acid sequence of avian thymic hormone, a parvalbumin. *Biochimie 72*, 653–660.
18. Serda, R. E., and Henzl, M. T. (1991) Metal ion-binding properties of avian thymic hormone. *J. Biol. Chem. 266*, 7291–7299.
19. Henzl, M. T., and Agah, S. (2006) Divalent ion-binding properties of the two avian *β*-parvalbumins. *Proteins 62*, 270–278.
20. Quay, S. C., and Condie, C. C. (1983) Conformational studies of aqueous melittin: thermodynamic parameters of the monomer-tetramer self-association reaction. *Biochemistry 22*, 695–700.
21. Henzl, M. T., and Graham, J. S. (1999) Conformational stabilities of the rat α- and *β*-parvalbumins. *FEBS Lett. 442*, 241–245.
22. Hapak, R. C., Lammers, P. J., Palmisano, W. A., Birnbaum, E. R., and Henzl, M. T. (1989) Site-specific substitution of glutamate for aspartate at position 59 of rat oncomodulin. *J. Biol. Chem. 264*, 18751–18760.
23. Haner, M., Henzl, M. T., Raissouni, B., and Birnbaum, E. R. (1984) Synthesis of a new chelating gel: removal of Ca^{2+} ions from parvalbumin. *Anal. Biochem. 138*, 229–234.
24. Henzl, M. T., Agah, S., and Larson, J. D. (2003) Characterization of the metal ion-binding domains from rat α- and *β*-parvalbumins. *Biochemistry 42*, 3594–3607.
25. Weber, G., and Young, L. (1964) Fragmentation of bovine serum albumin by pepsin. I. The origin of the acid expansion of the albumin molecule. *J. Biol. Chem. 239*, 1415–1423.
26. Schuck, P., Perugini, M. A., Gonzales, N. R., Howlett, G. J., and Schubert, D. (2002) Size-distribution analysis of proteins by analytical ultracentrifugation: strategies and application to model systems. *Biophys. J. 82*, 1096–1111.
27. Henzl, M. T., and Ndubuka, K. (2007) Low-affinity signature of the rat *β*-parvalbumin CD site. Evidence for remote determinants. *Biochemistry 46*, 23–35.
28. Daniel, E., and Weber, G. (1966) Cooperative effects in binding by bovine serum albumin. I. The binding of 1-aniline-8-naphthalenesulfonate. Fluorometric titrations. *Biochemistry 5*, 1893–1900.
29. Henzl, M. T., Davis, M. E., and Tan, A. (2008) Leucine-85 is an important determinant of divalent ion affinity in rat *β*-parvalbumin (oncomodulin). *Biochemistry 47*, 13635–13646.

30. Permyakov, E. A., Medvedkin, V. N., Korneichuk, G. A., Kostrzhevskaya, E. G., and Murzin, A. G. (1989) Binding of melittin to parvalbumin inhibited by Ca(II) ions. New function for parvalbumin. *Mol. Biol. (Moscow) 23*, 693–698.
31. Moorthy, A. K., Gopal, B., Satish, P. R., Bhattacharya, S., Bhattacharya, A., Murthy, M. R. N., and Surolia, A. (1999) Thermodynamics of target peptide recognition by calmodulin and a calmodulin analogue: Implications for the role of the central linker. *FEBS Lett. 461*, 19–24.
32. Henzl, M. T., Davis, M. E., and Tan, A. (2008) Divalent ion binding properties of the timothy grass allergen, Phl p 7. *Biochemistry 47*, 7846–7856.
33. Permyakov, S. E., Bakunts, A. G., Denesyuk, A. I., Knyazeva, E. L., Uversky, V. N., and Permyakov, E. A. (2008) Apo-parvalbumin as an intrinsically disordered protein. *Proteins 72*, 822–836.
34. van Holde, K. E., Johnson, W. C., and Ho, P. S. (2006) *Principles of Physical Biochemistry*, Pearson Prentice Hall, Upper Saddle River, NJ.
35. Cantor, C. R., and Schimmel, P. R. (1980) *Biophysical Chemistry*, W. H. Freeman, San Francisco.
36. Teller, D. C. (1976) Accessible area, packing volumes, and interaction surfaces of globular proteins. *Nature (London) 260*, 729–731.
37. Henzl, M. T., and Tanner, J. J. (2007) Solution structure of Ca^{2+}-free rat β-parvalbumin (oncomodulin). *Protein Sci. 16*, 1914–1926.
38. Henzl, M. T., and Tanner, J. J. (2008) Solution structure of the Ca^{2+}-free rat α-parvalbumin. *Protein Sci. 17*, 431–438.
39. Xie, D., and Freire, E. (1994) Structure based prediction of protein folding intermediates. *J. Mol. Biol. 242*, 62–80.
40. Hutnik, C. M. L., MacManus, J. P., and Szabo, A. G. (1990) A calcium-specific conformational response of parvalbumin. *Biochemistry 29*, 7318–7328.
41. Permyakov, E. A., Yarmolenko, V. V., Emelyanenko, V. I., Burstein, E. A., Closset, J., and Gerday, C. (1980) Fluorescence studies of the calcium binding to whiting (*Gadus merlangus*) parvalbumin. *Eur. J. Biochem. 109*, 307–315.
42. Strynadka, N. C. J., and James, M. N. G. (1989) Crystal structures of the helix-loop-helix calcium-binding proteins. *Annu. Rev. Biochem. 58*, 951–998.
43. Declercq, J. P., Tinant, B., Parello, J., and Rambaud, J. (1991) Ionic interactions with parvalbumins. Crystal structure determination of pike 4.10 parvalbumin in four different ionic environments. *J. Mol. Biol. 220*, 1017–1039.
44. Rada, J. A., and Denis, C. S. (2003) Analysis of gene expression during the recovery from experimental myopia. *Mol. Biol. Cell 14*, 367a.